A Numerical Assessment of Artificial Reef Pass Wave-Induced Currents as a Renewable Energy Source

Damien Sous

Journal of
Marine Science and Engineering

MDPI

Article

A Numerical Assessment of Artificial Reef Pass Wave-Induced Currents as a Renewable Energy Source

Damien Sous [1,2]

[1] Mediterranean Institute of Oceanography (MIO), Aix Marseille Université, CNRS, IRD, Université de Toulon, 13288 La Garde, France; sous@univ-tln.fr; Tel.: +33-(0)4-9114-2109

[2] Univ Pau & Pays Adour/E2S UPPA, Chaire HPC-Waves, Laboratoire des Sciences de l'Ingénieur Appliquées à la Méchanique et au Génie Electrique - Fédération IPRA, EA4581, 64600 Anglet, France

Received: 21 July 2019; Accepted: 19 August 2019; Published: 22 August 2019

Abstract: The present study aims to estimate the potential of artificial reef pass as a renewable source of energy. The overall idea is to mimic the functioning of natural reef–lagoon systems in which the cross-reef pressure gradient induced by wave breaking is able to drive an outward flow through the pass. The objective is to estimate the feasibility of a positive energy breakwater, combining the usual wave-sheltering function of immersed breakwater together with the production of renewable energy by turbines. A series of numerical simulations is performed using a depth-averaged model to understand the effects of each geometrical reef parameter on the reef–lagoon hydrodynamics. A synthetic wave and tide climate is then imposed to estimate the potential power production. An annual production between 50 and 70 MWh is estimated.

Keywords: artificial reef; positive energy breakwater; numerical simulation; turbines

1. Introduction

Low-lying nearshore areas host a significant and increasing population. Under the combined actions of sea level rise [1], modified storm patterns [2], and increasing urbanization, these regions will face growing risks of submersion, inundation, and erosion [3–6]. The preservation of the residential, economic, and ecological value of coastal regions will be a key issue in the decades and centuries to come. Nearshore management policies are increasingly relying on soft engineering approaches involving for instance managed retreat or artificial beach nourishment [7]. However, in a wide range of situations, hard-engineering artificial structures, generically called breakwaters, remain necessary to provide an effective protection from the incident wave energy and therefore to create safe berthing and navigation areas and to avoid erosion and submersion [8]. Continuous research efforts are engaged to optimize their performance in a wide range of meteo-marine conditions and to minimize their ecological impact.

Another major issue for the decades to come is the energy production in the context of climate change and population growth. A global effort is underway to extract renewable energy from marine sources, including kinetic energy from wind and currents, potential energy from tides, thermal potential, and osmotic pressure [9]. In addition, a number of devices, called wave energy converters (WEC), are being developed to extract energy from waves [10–13]. They include in particular oscillating wave surge converters [14], point absorber buoys [15], oscillating water column [16], overtopping devices [17], or, more recently, pressure differential systems [18]. While increasing research and technological efforts are spent to improve their efficiency, most of them are based on the direct extraction of the mechanical energy of waves which causes a range a problem in terms of mechanical complexity and sustainability.

The present study aims to propose a new perspective in the combined issues of nearshore protection and energy production [17,19–22]. The guiding framework is to provide a novel insight on the development of artificial structures primarily designed as breakwaters, i.e., to shelter the coast from waves impact while accounting for ecological issues, but also, as a secondary requirement, to produce energy. Such an approach can be synthesized under the concept of positive energy breakwater (PEB). The idea is here to evaluate the potential of a specific nature-based solution, aiming to mimic the mechanisms involved over coral barrier reefs. In nature, wave breaking on barrier reefs induces a barotropic cross-shore component of current resulting from the depth-averaged balance between the gradient of radiation stress, the bottom friction, and the horizontal surface (setup) gradients [23–29]. Using cross-reef wave-induced current rather than directly extracting energy from wave motions has the main advantage of allowing the use of well-developed and robust technologies such as river turbine generators and to avoid the implementation of complex articulated and/or floating devices. However, on the other hand, less overall mechanical energy should be available due to breaking and frictional losses when compared to a direct extraction in the wave field. The present study aims to provide a first assessment of the energy production that can be expected from a reef-mimicking PEB.

The general trend of cross-reef current is that, as soon as breaking occurs, the current increases with wave height and water level [29,30]. The cross-reef current is therefore constantly evolving in response to the variations of incoming wave energy and the fluctuations of still water level under the effect of tide and other large scale oscillations. The objective of the present paper is two-fold. First, a series of wave-resolving numerical simulations is performed to evaluate the hydrodynamical functioning of a PEB mimicking the coupled wave-circulation dynamics of coral reef-barrier systems. The core issue is to discuss the PEB design not only for given conditions of waves and water level but for a more realistic climate. Then, based on a selected design and a synthetic wave and tide climate, a first annual estimate of the power potential will be carried out.

2. Methods

2.1. Numerical Model

Several strategies have been used to model the hydrodynamics above reefs. Once fitted on field data, empirical [30] or analytical [26–28,31] models are able to provide correct orders of magnitude for cross-reef currents and transports in very open systems, i.e., when the reef can be considered nearly isolated in a hydrodynamical point of view. In the presence of a well-developed reef–lagoon system, the topobathymetric constraints applied by the lagoon boundaries can significantly affect the overall hydrodynamics in terms of circulation and water levels [32] depending on the degree of closure of the whole system. Such feedback on the reef hydrodynamics requires to run more complex wave-circulation numerical models. In the last decade, both short-wave-averaged models such as XBeach [33–35] or phase-resolving simulations using nonhydrostatic models such as SWASH [35–37] or Boussinesq-type models [38–40] have been successfully used to model wave transformation and/or related lagoonary circulation. In the present case, the first aim is to get a simple and robust view of the overall hydrodynamics of the system. The present study will therefore be based on the coupled wave-circulation XBeach model [41]. The mean flow is computed from the shallow water equations using the depth-averaged Generalized Lagrangian Mean [42] formulation. In this equation system, the basic momentum equation includes inertial, Coriolis, bottom friction, wind stress, horizontal diffusion, and surface slope terms formulated in terms of the Lagrangian velocity defined as the sum of the Eulerian velocity and Stokes drift. The directional and time-dependent wave force is further included in this equation using a wave action equation [43] associated with a roller energy equation for wave dissipation. In the case of stationary waves used in the present study, the wave breaking dissipation is based on the Janssen and Battjes [44] formulation. Note that the effect of the outward flow in the pass can have a significant effect on the incident wave field. Xbeach takes into account this effect by

correcting the wave number with the use of Eikonal equations, therefore modifying the group and phase velocities speed.

The code is used here in its simpler stationary configuration, all model parameters being kept to default values unless mentioned otherwise. No morphological evolution is allowed. For each simulation, 5-min stationary frontal wave runs are performed, with outputs being extracted at the end of the computation.

2.1.1. Cross-Shore Benchmark Case

A first validation study is carried out on a purely cross-shore configuration of the model. The main aim is to check the ability of the numerical model to represent the depth-averaged momentum balance along a barrier reef. In particular, it is of primary importance to determine the performance of the model in the description of wave breaking above the reef and the consequent production of cross-reef current induced by wave-induced pressure gradient. The validation data has been recovered during a dedicated in situ experimental campaign on the Ouano reef, New Caledonia. This site has been selected for benchmarking in the present study because it is a large channel lagoon where waves are by far the main driver of the reef hydrodynamics. This means that, on the barrier reef, the tide effect and the lagoon boundaries can be neglected as soon as the waves are large enough to break [45]. The deployed instrumentation and the field site are presented in details in Sous et al. [29]. The complete numerical domain is 2500 m long, ranging from $X = -500$ to 2000 m with a 5 m uniform resolution (X is the cross-shore abscissa). A zoomed view of the bathymetric profile is given in Figure 1, upper plot, the open ocean and lagoon being on left and right sides, respectively. The numerical simulations are forced with reef-normal wave conditions encountered on 29 May 2016 at 15:40. Deep water significant wave height and period are 2.44 m and 11.4 s. Still water level is imposed at 0.53 m according to the measurements performed outside the wave action zone [29]. The only calibrating parameters are the wave and mean current friction coefficients. They are imposed at 0.5 and 0.03, respectively, in order to mimic the high roughness of coral reefs [34].

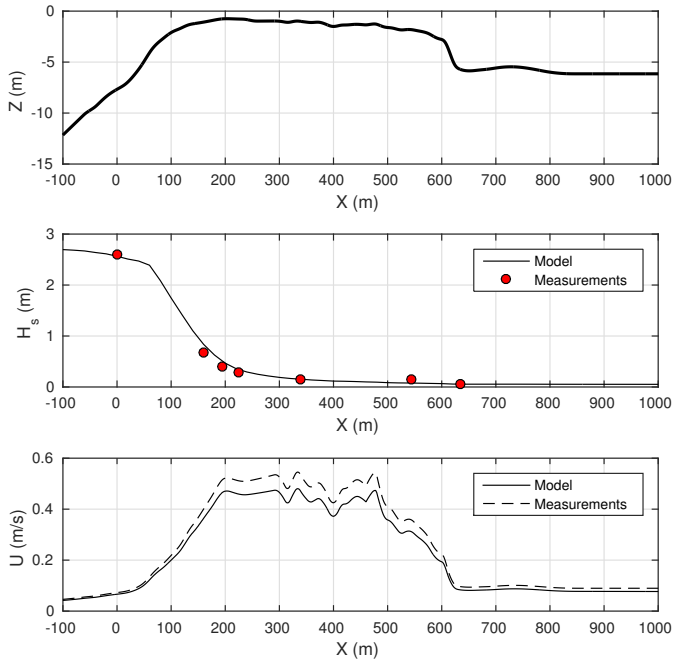

Figure 1. Confrontation between numerical prediction and in situ measurements on the Ouano barrier reef, New Caledonia. Waves are coming from the open ocean, at the left side. Top panel: bed elevation. Middle panel: cross-shore profile of significant wave height. Bottom panel: cross-shore profile of depth-averaged velocity.

The simulated significant wave height along the full profile is compared in Figure 1 (middle plot) with the measurements performed by bottom-moored pressure sensors over the barrier. The cross-shore velocity driven by wave breaking is compared to the point measurements performed with a single acoustic Doppler velocity profiler deployed at $X = 630$ m, and further extrapolated across the complete cross-shore profile assuming the conservation of transport. The numerical results are very satisfactory both in terms of reproduction of both the cross-shore wave profile, with a strong attenuation due to wave breaking, and the cross-shore velocity. Corresponding RMS errors are 5.6 cm and 2.5 cm/s. These combined observations ensure the accurate reproduction of the depth-averaged momentum balance across the barrier reef. These good results have been obtained against field data in a widely open reef–lagoon system. This allowed validating the production of wave-induced cross-shore current, which is the main driver of the smaller and more closed artificial reef–lagoon systems studied hereafter.

2.1.2. Artificial Breakwater Configurations

The model is then used in a series of 2D configurations to explore the hydrodynamical functioning of complete artificial breakwater–lagoon systems. The reference computational domain is 500 and 2000 m long in cross- and alongshore directions, respectively, with 10-m uniform horizontal resolution. The base bathymetry is an along-shore uniform linear slope ($\tan\beta = 0.022$), with bed elevation ranging from -10 to 1 m from offshore to beach boundaries. Note that the domain is extended in cross-shore direction in Section 3.2.2 in order to simulate case of breakwaters further offshore. A range of synthetic breakwaters is imposed over this base bathymetry; all of which are made of two symmetric wings separated by a pass. The geometrical parameters are defined as follows (see Figure 2).

- W is the width of the reef pass
- $L1$ is the distance from the shore to the reef pass
- $L2$ is the length of each wing
- α is the breakwater angle
- D is the breakwater width
- H is the breakwater top depth, which is constant for a given case.

The reference reef geometry is depicted in Figure 2, based on the following values; $W = 60$ m, $L1 = 200$ m, $L2 = 300$ m, $\alpha = 0.1$, $H = 1$ m, and $D = 100$ m.

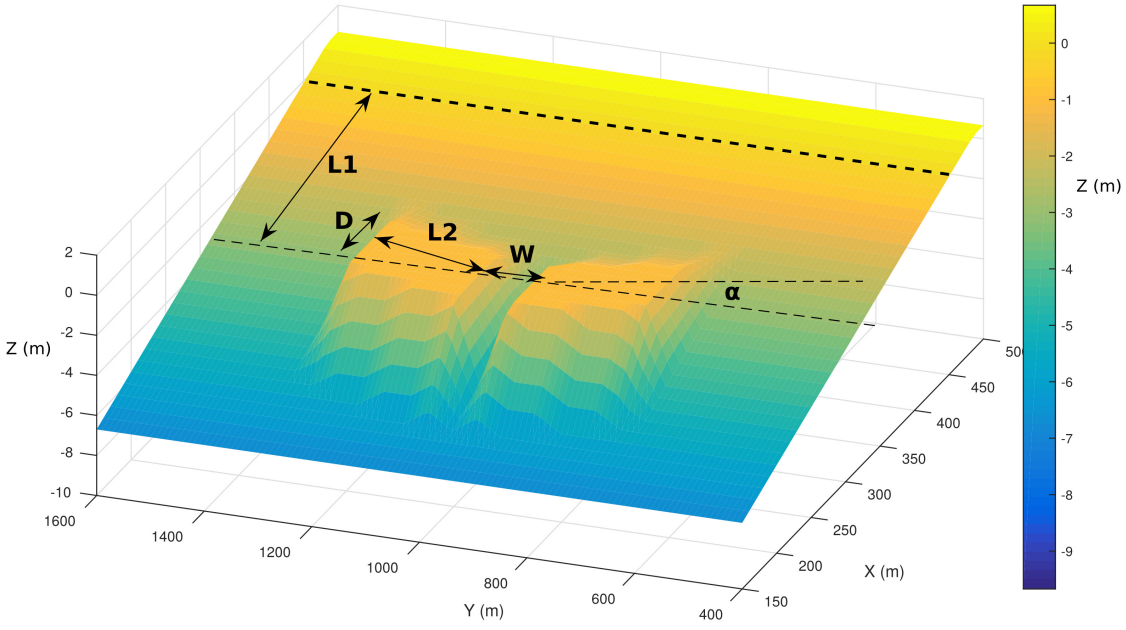

Figure 2. Numerical bathymetry and geometrical parameters.

The forereef slope is approximately $\tan\beta = 0.04$. A part of the incoming wave energy can be reflected over the forereef, in particular for low water level. This effect is not represented by the present numerical model and would require more sophisticated approaches. However, following existing field [46] and laboratory [47] observations of moderate wave reflection on similar systems, one can expect that the effect on the overall dynamics remains small.

2.2. Strategy

Wave breaking dynamics, which is the main driver of the overall system, is primarily dependent on the wave height to depth ratio. Consequently, the effects of the distance to the shore, $L1$, and the reef top depth, H, are strongly related to the imposed wave climate and tidal elevation. The optimization procedure for the set of breakwater parameters is therefore twofold. First, a single reference wave case with wave height and period of 1.8 m and 12 s, respectively, is used to analyze the effect of W, $L2$, α, and D, see Section 3.1.3. This energetic reference condition can be for instance considered as representative of the southeast Bay of Biscay climate [48,49]. A more complete wave climate is then applied to optimize $L1$ and H, see Section 3.2.

2.3. Power Estimation

The power estimation is based on the assumption of a network of underwater turbines deployed at the sea bottom across the pass between breakwater wings. A diversity of river and marine turbines may be implemented for such an application. For the present study, typical features of the turbine Poseide P154® from Guinard Energies are used. The power output for a single turbine is typically of the order of 750 U^3 W, where U is the mean velocity. The turbine diameter is ~2.3 m. For the present estimation, the assumption is made that a turbine can be implemented each 3 m along the cross-section of the reef pass, i.e., the number of turbines is the integer portion of $W/3$. Note that a minimal velocity of 0.8 m·s^{-1} is imposed for the turbine to start producing energy, i.e., a zero production is assumed for lower velocity.

3. Results

3.1. Reference Case

3.1.1. Basic Reef Hydrodynamics

The basic hydrodynamics of the reef–lagoon system is depicted in Figure 3 for the reference case. The wave forcing is shore normal and stationary and propagates from the left to the right. The effect of the breakwater on the wave dynamics is straightforward, see Figure 3A. It first induces a short shoaling from $X = 220$ m over the forereef slope, followed by a strong decrease of wave height due to breaking above the reef edge and on the reef flat. Behind the breakwater, waves enter the lagoon with a strongly reduced amplitude, typically 25% of the offshore incoming height and further propagate toward the shore. Strong horizontal gradients develop in the wave field, both cross-shore on both sides on the breakwater and alongshore between sheltered and free areas. The breakwater effect is also clearly identified on the mean water level. The gradient of radiation stresses in the breaking zone induces a barotropic pressure gradient leading to an increase of the mean water level in the breaking zone, the so-called wave setup [50]. However, by contrast to the classical beach case, the submerged barrier reefs are characterized by an open boundary at the end of the breaking zone. This allows the development of a cross-shore current which tends to fill the lagoon. In the present simulation, the cross-reef current reaches ~1.5 m·s^{-1} above the breakwater (Figure 3D). The whole reef–lagoon system is therefore driven by an overall depth-averaged momentum balance involving the gradient of radiation stress, the surface gradient and the friction. This balance is further constrained by the system topography [32]. The frictional resistance on the output flows through the central reef pass and on the lateral exits induces a significant wave setup inside the coastally bounded

lagoon. Any modification in the breakwater geometry and positioning is thus expected to affect wave breaking process, surface gradients, and flow resistance across the entire system. The estimation of the magnitude of the return flow in the reef pass requires therefore the resolution of the momentum balance over the whole breakwater/lagoon system.

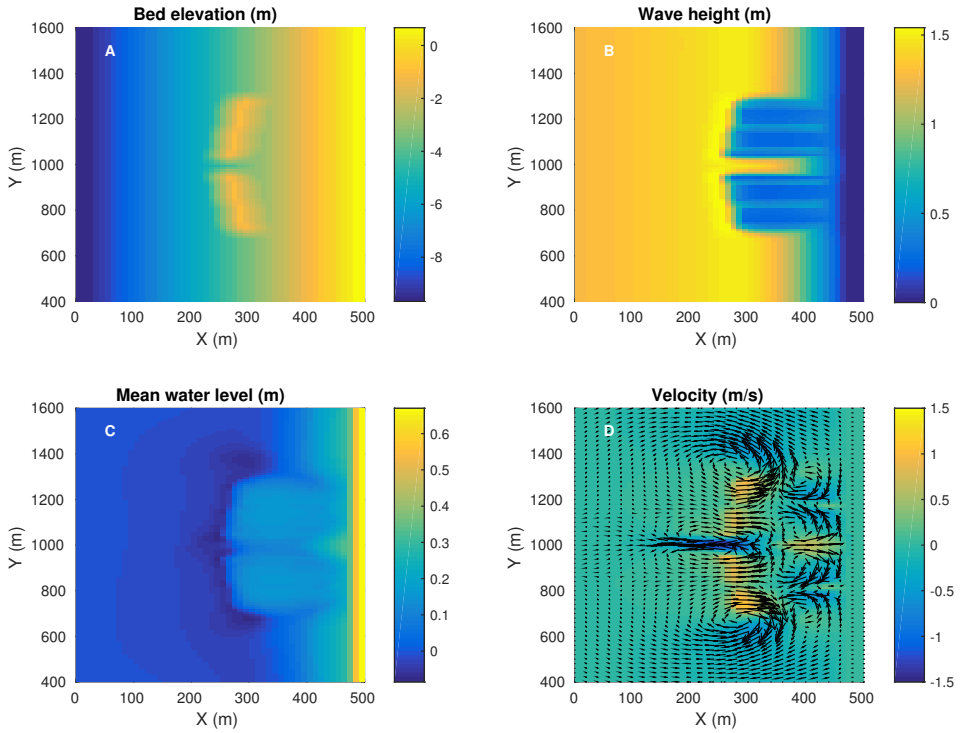

Figure 3. Reference case hydrodynamics. (**A**) Bed elevation. (**B**) Wave height. (**C**) Mean water level. (**D**) Contour of cross-shore velocity and velocity vectors field (only one fourth of the computational points are shown). Positive velocity correspond to onshore directed flow.

3.1.2. Side Wall Effect

The return flow is directly dependent on cross-shore pressure gradient through the pass driven by the mean water setup within the lagoon. This latter should a priori be enhanced by limiting or closing the lateral openings of the lagoon. A new configuration is tested by adding lateral emerging walls on the Reference case, all other parameters being kept constant. Figure 4 shows the resulting velocity fields. The effect of lateral walls is straightforward. A new overall balance is observed with two contrasting effects. By stopping the lateral output flows, the only exiting flow is in the reef pass which thus tends to increase. On the other hand, this results in a higher mean water level in the lagoon which limits the cross-shore flow above the breakwater. Consequently, the reduction of wave breaking-induced flux toward the lagoon induces a decrease of the output flow in the pass. For the present case, the net effect on the reef pass output is positive, with a slight increase of the offshore-directed velocity from 1.45 to 1.5 $m \cdot s^{-1}$. This results in a increase of estimated power production from 46 to 51 kW, compared to the no side walls case. However, the balance between the two aforementioned effects may not be systematically positive in terms of power production. In order to get a comprehensive view of the effect of side walls for a range of reef geometry, both with- and without walls configurations will be tested when exploring the effect of W, $L2$, α, and D in the following section.

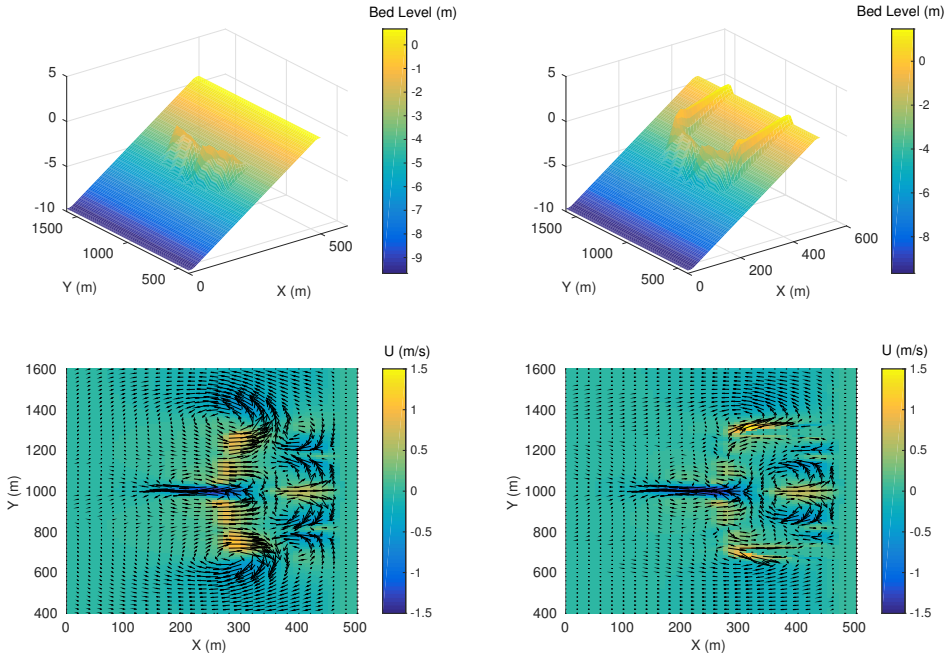

Figure 4. Side walls effect.

3.1.3. Parameters Optimization

Figure 5 shows the effect of four breakwater parameters on the computed power production: the breakwater angle α (Figure 5A), the breakwater length $L2$ (Figure 5B), the breakwater width D (Figure 5C), and the reef pass width W (Figure 5D). For each parameter, a range of value is tested with and without sidewalls in black and red lines, respectively.

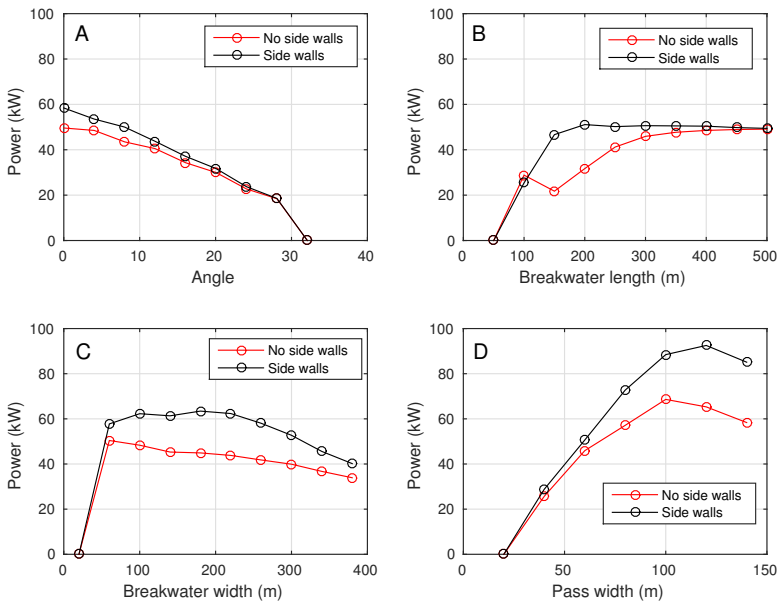

Figure 5. Power production for four parameters, with and without side walls. (**A**) Breakwater angle. (**B**) Breakwater length. (**C**) Breakwater width. (**D**) Reef pass width.

The role of breakwater angle (Figure 5A) is monotonic: the lower the angle, the stronger the power production. This indicates that reef-normal wave exposure produces the higher output in the pass. This result can also be interpreted, at least qualitatively, as an estimation of the effect of wave incidence. For angle greater than 20°, the power production is reduced by half. For angle greater than 30°, the power production becomes nearly negligible. The effect of side walls increases the power by ~20%.

The effect of breakwater length is rather asymptotic (Figure 5B). In the presence of side walls, the power production increases rapidly with $L2$ until a nearly constant power is obtained for $L2 > 200$ m. Without side walls, the behavior is more complex for small $L2$. The production increases slower with $L2$ than with side walls. The asymptotic value is obtained for $L2 > 450$ m, i.e., nearly twice the breakwater length required to produce the same power with side walls.

A minimal width of ~50 m is required to turn on the energy production (Figure 5C). This corresponds to the minimal breakwater width allowing a fully developed breaking zone. The trend depends on the presence of side walls. With side walls, a nearly constant and maximal production is obtained for $100 < W < 250$ m and then slowly decreases with increasing W. Without side walls, the maximal production is reached for $W = 60$ m, and then constantly decreases with W.

The effect of pass width D (Figure 5D) depends on the combination of the intensity of the return flow and the pass cross-section which allowed to deploy more turbines (see Section 2.3). The net result in terms of power production is that the production first increases with D until a maximal value is reached about $D = 100$ and 120 m for walls and no walls cases, respectively. For larger reef pass, the production is observed to drop. The underlying process is that, above a width pass larger than 120 m, the increase of power due to the larger available section for turbine deployment is overwhelmed by the decrease of outflow velocity: the power production is a linear function of the turbine number but depends on the cubed velocity. The effect of side walls is here to increase the production up to 50%.

The first phase of optimization provides the following set of values for the base parameters: $L2 = 200$, $W = 100$, and $D = 120$ m. For the angle, a value of 10° is chosen in order to work with a more realistic case than a perfectly reef-normal wave incidence. This first level of optimization case will be referred hereafter as Opti1 case. $L1$ and H will be first kept to the reference values to understand the effect of wave and tide conditions (Section 3.2.1) on Opti1 and then adjusted on a synthetic wave climate (Section 3.2.2) to provide Opti2 reef geometry. In each tested configurations, the presence of side walls allowed a moderate to significant increase of production. Consequently, side walls will be imposed in the breakwater configuration for the following analysis.

3.2. Dependency on External Forcings

The power production is directly related to the wave breaking. This process is widely controlled by the ratio between wave height and local depth. Such dependency involves the incoming wave height, the tide level, the breakwater top depth H and the distance to the shore $L1$ (in the idealized case of a linear bathymetry). The role of wave height and tide are first explored on Opti1 case. Then a synthetic wave and tide climate is simulated to provide optimized values for H and $L1$.

3.2.1. Wave and Tide Effect

Figure 6 depicts the effect of incoming wave height, wave period and still water level (SWL) on the Opti1 power production. For small wave height (>1 m), no production is observed. In this case, wave breaking is either absent or too weak to generate sufficient gradient in radiation stress to drive the whole system in circulating pattern. Then the power production strongly increases with wave height. The maximum value is reached ~2.1 m. For larger incoming waves, the breaking point is shifted offshore. Part of the wave energy is dissipated before the forereef which results in a lower wave setup over the reef top and a lower output flow. This trend increases when increasing wave height. The effect of wave period is straightforward: the longer the wave, the higher the power. This is directly related to the increase of incoming wave energy for longer waves, which induces, after conversion into

kinetic energy by the reef–lagoon system, a higher output flow. The effect of tide is directly related to the breaking process and the reef submersion. For low SWL, the reef is emerging and acts as a closed boundary which inhibits any circulation. From SWL$= -1.2$ m, the reef top is progressively submerged. Breaking waves are able to induce wave setup and circulation can develop. The output flow thus results from the momentum balance of the whole system. It increases with water level until a maximal value which is reached for SWL about 0 and thus decreases. For SWL greater than 0.8 m, the water depth above the reef top is larger than the critical breaking depth and waves can propagate without breaking across the breakwater.

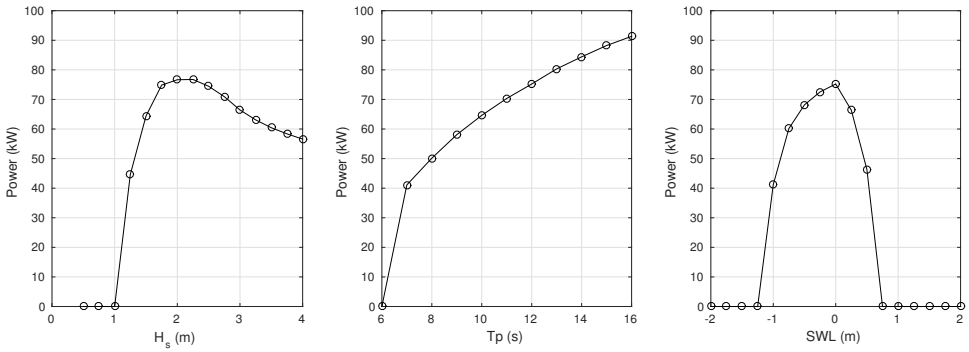

Figure 6. Effect of wave height, period and still water level on power production for Opti1 case.

3.2.2. Optimization for an Annual Synthetic Climate

The previous results demonstrate the connected effects of wave height, tide level, reef top depth, and breaking point location with respect to the breakwater position on the power production. A synthetic wave and tide climate is now simulated to gain insight on the role of H and $L1$. Five wave conditions are considered with the following height/period parameters; 0.5/6, 1/8, 1.5/10, 2/12, 3/14, and 5 m/15 s. The respective occurrences for each wave climate are 10%, 20%, 3%, 25%, 10%, and 5%. This wave climate, which is quite energetic, is inspired from the wave statistics of the southeast Bay of Biscay [48,49]. The computational procedure is the following. A tidal cycle is divided into N_t tidal steps. For the present case, the tidal range is from -2 to 2 m and $N_t = 5$, i.e., 1 m tidal steps. For a given wave climate, an individual power P_i is first computed on each tidal step. Assuming a semidiurnal tide with a single M2 component, the energy production over a tidal cycle is the sum of $E_t = 12.42 P_i N_t$. The daily energy production for a given wave climate is, therefore, $E_d = \frac{24}{12.42} E_t$. Finally, the annual energy production is computed as the annual sum of each of the six wave climate weighted by their respective occurrences.

The complete calculation is thus performed for a range of reef top depth H from 0 to 3 m with 0.5 m steps and distance to shoreline $L1$ from 100 to 700 m with steps of 50 m. The total number of simulated cases is thus 1225. The results are depicted in Figure 7, left. The annual energy production strongly depends non-monotonically on both reef top depth and distance to the shoreline. The maximal output for the selected wave climate is obtained for H and $L1$ values of approximately 2 and 500 m, respectively. It reaches 70 MWh, but can drastically be reduced when varying the breakwater location and/or depth.

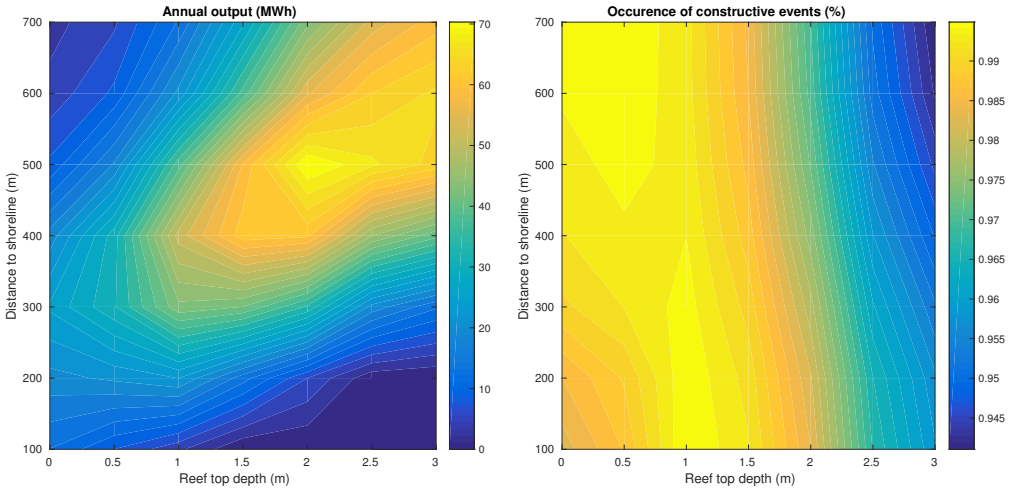

Figure 7. (**Left**) Annual energy production for a synthetic wave and tide climate versus reef top depth and distance to the shoreline. (**Right**) Annual occurrence of constructive conditions versus reef top depth and distance to the shoreline.

3.2.3. Beach Protection

Beach protection is a very rich and complex topic that involves a number of hydrodynamical and morphological processes. The first aim here is to identify the extent to which the breakwater optimization for power production is compatible or conflicting with the beach protection issue. The approach is to divide wave conditions into two classes: constructive or destructive [51]. A simple *a priori* threshold is taken here at 1.5 m for wave height just after the breakwater: cases with wave height lower than 1.5 m are called as constructive. A annual occurrence of constructive conditions is calculated to provide an estimate of the sheltering effect provided by a given breakwater configuration. This parameter is expected to be mainly controlled by the dynamics of wave breaking which primarily involves wave height, tide level, reef top depth and breakwater cross-shore position. Similarly to the previous section for the optimization of H and $L1$, a global analysis is performed on an annual wave and tide climate, see Figure 7B. The first observation is the relatively small variation of the occurrence of constructive events, which ranges from 94.5 to 99.5%. However, damages on beach systems are usually caused by a small number of strong to extreme wave events. It is therefore expected that a small difference in occurrence of constructive events leads to major difference in beach exposure to damaging conditions. The depth effect is straightforward: the shallower the reef, the stronger the wave attenuation, the better the protection. The role of breakwater cross-shore location is much weaker. Comparing Figure 7A,B, one notes the absence of relationship between energy protection and beach protection. A best compromise has therefore to be found. For instance, in the present wave climate, H and $L1$ values of approximately 1.5 and 450 m should promote energy production above 50 MWh while maintaining constructive events above 98%.

4. Discussions

The present numerical study aims to provide a first quantitative insight on the potential of energy production by wave breaking driven return flow in artificial breakwater system. The study has been carried out on a series of idealized cases, in order to get a straightforward understanding of the physical processes driving the hydrodynamics of the whole system and the consequences in terms of energy production. The first results demonstrate that for a breakwater system occupying about 500 m along the shore, an annual energy protection of the order of 50 to 70 MWh may be envisioned. Such values are comparable to the power typically harvested with river turbine systems [52,53]. For a single breakwater–lagoon system, such values are about one fourth of the already operating

Mutriku wave farm [54] or Azura wave power generator [55]. Multiplying the number of devices along a well-developed shoreline will naturally allow to increase the power production and reach the expected harvesting for large scale ongoing wave farm projects such as Agucadoura (Portugal), Orkney (UK) or Sotenas (Sweden) or large tidal current turbines [56].

However, these comparisons in terms of energy harvesting should account for the fundamental differences between systems. The present prospect supports the concept of Positive Energy Breakwater (PEB). The primary objective is to keep the fundamental role of immersed breakwater, i.e., to maintain and enhance beach resilience to wave events by promoting constructive wave conditions and filtering out damaging events. This sheltering effect also promotes a lagoon-like functioning of the nearshore system, with enhanced attractivity for navigational, residential, and recreational purposes. In addition to this baseline, the idea stated here is to use the breakwater structure to produce energy with a simple river-like turbine system. This PEB concept has therefore to be considered as a whole. In particular, the design optimization needs to be carried out for a selected site with given bathymetry and wave and tide conditions, taking into account all the local social, ecological, and economic constraints.

In a more realistic configuration, a number of issues are expected to affect the functioning of the system. Every cases can obviously not be tested here and specific analysis would be needed on each envisioned configuration. On a purely hydrodynamical point of view, the depth-averaged approach followed here is not able to take into account the vertical structure of the flow. Significant shear may be present in the output flow through the pass, in particular considering the presence of turbines deployed near the bottom. Combined with the complex interactions with the wave field in this zone, this calls for higher resolution (2DV or 3D) models allowing to take into account the full flow structure, better understand the wave-current interaction in the context of a vertically sheared current, and evaluate the optimal positioning and design of turbines in the water column. The bottom friction needs also to be accounted for more carefully. In the present study, a constant bottom friction coefficient is applied. The default XBeach value of 0.003 (mean flow friction) is used, which corresponds to a uniformly smooth bed. One may expect that artificial structures with large roughness will significantly alter the overall hydrodynamics by slowing down the overall circulation and increasing wave dissipation. Similarly, the additional drag induced by the turbines row has been neglected in the present study. This effect can not be evaluated independently of the hydrodynamical functioning of the whole reef–lagoon system and will require more sophisticated numerical approaches. Keeping the simple depth-averaged modeling used here, indicative tests have been performed to include an additional drag force in the breakwater pass via an increase of the bottom friction coefficient. Imposing a value of 0.03 in the pass instead of the default 0.003 value all across the pass induces an overall decrease of the circulation in the system, with a reduction about 7% of the output velocity (23% in power production). The role of wave incidence is also important, as demonstrated by Figure 6A, and the breakwater needs to be designed accounting for mean wave direction. More generally, the wave climate and tidal conditions are both essential drivers of the system. For a selected site, the design optimization and the estimation of energy production must be assessed with a careful consideration of wave and tide conditions.

The underlying bathymetry is also of primary importance. In the majority of cases, the shoreface shape will show significant discrepancies from the linear alongshore-uniform profile used here, with the presence of a wide range of morphological structures. The breakwater design needs to be adapted to the local bathymetry and its evolution. In addition, the implementation of such artificial structure will have important impact on the beach morphodynamics [57,58]. These issues, which are outside of the scope of the present paper, also need to be addressed with care.

Finally, it is emphasized that the optimization procedure for the breakwater dimensions and positioning relies here mainly on an individual parameter optimization for a fixed ensemble geometry. A comprehensive optimization of breakwater system on a realistic initial bathymetry with no a priori geometry [51,59] may lead to significantly different designs likely able to increase energy production. This optimization should be carried out accounting for engineering perspectives, aiming to globally

minimize the overall quantity of building material. For instance, a minimal breakwater ~60 m wide is suggested by the present study to allow the development of a full breaking zone (see Figure 5C), but further efforts should be spent to identify the optimal width for a given site.

5. Conclusions

The present study aims to assess, via a series of numerical simulations, the potential of artificial reef pass wave-induced current as a renewable energy source. The depth-averaged wave-circulation model is based on the XBeach open source code. The model is first validated in a purely cross-shore configuration against field data recovered on coral barrier reef system in order to ensure the accurate representation of wave breaking-induced current which is the fundamental driver of the whole system. A series of numerical simulations is then carried out to understand the role of the geometrical parameters of the artificial reef–lagoon system on the power potential for a reference wave case. A synthetic wave and tide climate is finally applied on the optimized artificial reef to estimate the annual power production. A production ranging between 50 and 70 MWh is reached for an artificial breakwater–lagoon system extending ~500 m in cross-shore and along-shore directions, the breakwater top being ~1m below the still water level. Together with the beach sheltering effect provided by such system, this amount of power production should make the considered system a promising option for marine renewable energy production.

The present study has been carried out on an idealized system in order to understand the fundamental functioning. The next step toward an operational prospect is the application to a realistic site. The approach proposed here, based on a simple and robust depth-averaged wave-circulation numerical model, can be kept and used on real bathymetric data and wave and tide statistics to confirm the system performance. After ensuring that an efficient compromise can be reached between energy production and beach protection using the present method for a selected site, an extensive study coupling local engineering, morphodynamical, economical, and ecological issues will be undoubtedly required.

Funding: This research received no external funding

Acknowledgments: The author is grateful to Guinard Energies for providing turbine power curve data.

Conflicts of Interest: The author declares no conflicts of interest.

References

1. Hay, C.C.; Morrow, E.; Kopp, R.E.; Mitrovica, J.X. Probabilistic reanalysis of twentieth-century sea-level rise. *Nature* **2015**, *517*, 481. [CrossRef] [PubMed]
2. Hansen, J.; Sato, M.; Hearty, P.; Ruedy, R.; Kelley, M.; Masson-Delmotte, V.; Russell, G.; Tselioudis, G.; Cao, J.; Rignot, E.; et al. Ice melt, sea level rise and superstorms: Evidence from paleoclimate data, climate modeling, and modern observations that 2 C global warming could be dangerous. *Atmos. Chem. Phys.* **2016**, *16*, 3761–3812. [CrossRef]
3. Brown, A.; McLachlan, A. Sandy shore ecosystems and the threats facing them: Some predictions for the year 2025. *Environ. Conserv.* **2002**, *29*, 62–77. [CrossRef]
4. Defeo, O.; McLachlan, A.; Schoeman, D.S.; Schlacher, T.A.; Dugan, J.; Jones, A.; Lastra, M.; Scapini, F. Threats to sandy beach ecosystems: A review. *Estuar. Coast. Shelf Sci.* **2009**, *81*, 1–12. [CrossRef]
5. Schlacher, T.A.; Schoeman, D.S.; Dugan, J.; Lastra, M.; Jones, A.; Scapini, F.; McLachlan, A. Sandy beach ecosystems: Key features, sampling issues, management challenges and climate change impacts. *Mar. Ecol.* **2008**, *29*, 70–90. [CrossRef]
6. Semeoshenkova, V.; Newton, A. Overview of erosion and beach quality issues in three Southern European countries: Portugal, Spain and Italy. *Ocean Coastal Manag.* **2015**, *118*, 12–21. [CrossRef]
7. Phillips, M.R.; Jones, A.L. Erosion and tourism infrastructure in the coastal zone: Problems, consequences and management. *Tour. Manag.* **2006**, *27*, 517–524. [CrossRef]

8. Kamphuis, J.W. *Introduction to Coastal Engineering and Management*; World Scientific: Singapore, 2010; Volume 30.
9. Mueller, M.; Wallace, R. Enabling science and technology for marine renewable energy. *Energy Policy* **2008**, *36*, 4376–4382. [CrossRef]
10. López, I.; Andreu, J.; Ceballos, S.; de Alegría, I.M.; Kortabarria, I. Review of wave energy technologies and the necessary power-equipment. *Renew. Sustain. Energy Rev.* **2013**, *27*, 413–434. [CrossRef]
11. Combourieu, A.; Lawson, M.; Babarit, A.; Ruehl, K.; Roy, A.; Costello, R.; Laporte Weywada, P.; Bailey, H. *WEC3: Wave Energy Converter Code Comparison Project: Preprint*; Technical Report; National Renewable Energy Laboratory (NREL): Golden, CO, USA, 2017.
12. Ozkop, E.; Altas, I.H. Control, power and electrical components in wave energy conversion systems: A review of the technologies. *Renew. Sustain. Energy Rev.* **2017**, *67*, 106–115. [CrossRef]
13. Mustapa, M.; Yaakob, O.; Ahmed, Y.M.; Rheem, C.K.; Koh, K.; Adnan, F.A. Wave energy device and breakwater integration: A review. *Renew. Sustain. Energy Rev.* **2017**, *77*, 43–58. [CrossRef]
14. Henry, A.; Folley, M.; Whittaker, T. A conceptual model of the hydrodynamics of an oscillating wave surge converter. *Renew. Energy* **2018**, *118*, 965–972. [CrossRef]
15. Franzitta, V.; Catrini, P.; Curto, D. Wave energy assessment along Sicilian coastline, based on DEIM point absorber. *Energies* **2017**, *10*, 376. [CrossRef]
16. Rezanejad, K.; Soares, C.G.; López, I.; Carballo, R. Experimental and numerical investigation of the hydrodynamic performance of an oscillating water column wave energy converter. *Renew. Energy* **2017**, *106*, 1–16. [CrossRef]
17. Contestabile, P.; Iuppa, C.; Di Lauro, E.; Cavallaro, L.; Andersen, T.L.; Vicinanza, D. Wave loadings acting on innovative rubble mound breakwater for overtopping wave energy conversion. *Coast. Eng.* **2017**, *122*, 60–74. [CrossRef]
18. Algie, C.; Ryan, S.; Fleming, A. Predicted power performance of a submerged membrane pressure-differential wave energy converter. *Int. J. Mar. Energy* **2017**, *20*, 125–134. [CrossRef]
19. Vicinanza, D.; Stagonas, D.; Müller, G.; Nørgaard, J.H.; Andersen, T.L. Innovative breakwaters design for wave energy conversion. *Coast. Eng. Proc.* **2012**, *1*, 1. [CrossRef]
20. Vicinanza, D.; Contestabile, P.; Di Lauro, E. Overtopping Breakwater for Wave Energy Conversion: Status and Perspective. In Proceedings of the 12th European Wave and Tidal Energy Conference, Cork, Ireland, 27 August–1 September 2017; Volume 27, pp. 1194-1–1194-9.
21. Zhang, X.; Zeng, Q.; Liu, Z. Hydrodynamic Performance of Rectangular Heaving Buoys for an Integrated Floating Breakwater. *J. Mar. Sci. Eng.* **2019**, *7*, 239. [CrossRef]
22. Rosa-Santos, P.; Taveira-Pinto, F.; Clemente, D.; Cabral, T.; Fiorentin, F.; Belga, F.; Morais, T. Experimental Study of a Hybrid Wave Energy Converter Integrated in a Harbor Breakwater. *J. Mar. Sci. Eng.* **2019**, *7*, 33. [CrossRef]
23. Lowe, R.J.; Falter, J.L.; Bandet, M.D.; Pawlak, G.; Atkinson, M.J.; Monismith, S.G.; Koseff, J.R. Spectral wave dissipation over a barrier reef. *J. Geophys. Res. Ocean.* **2005**, *110*, 1–16. [CrossRef]
24. Monismith, S.G. Hydrodynamics of coral reefs. *Annu. Rev. Fluid Mech.* **2007**, *39*, 37–55. [CrossRef]
25. Lugo-Fernández, A.; Roberts, H.; Wiseman, W., Jr.; Carter, B. Water level and currents of tidal and infragravity periods at Tague Reef, St. Croix (USVI). *Coral Reefs* **1998**, *17*, 343–349. [CrossRef]
26. Hearn, C.J. wave breaking hydrodynamics within coral reef systems and the effect of changing relative sea level. *J. Geophys. Res. Ocean.* **1999**, *104*, 30007–30019. [CrossRef]
27. Gourlay, M.R.; Colleter, G. Wave-generated flow on coral reefs—An analysis for two-dimensional horizontal reef-tops with steep faces. *Coast. Eng.* **2005**, *52*, 353–387. [CrossRef]
28. Bonneton, P.; Lefebvre, J.P.; Bretel, P.; Ouillon, S.; Douillet, P. Tidal modulation of wave-setup and wave-induced currents on the Aboré coral reef, New Caledonia. *J. Coast. Res.* **2007**, *50*, 762–766.
29. Sous, D.; Tissier, M.; Rey, V.; Touboul, J.; Bouchette, F.; Devenon, J.L.; Chevalier, C.; Aucan, J. Wave transformation over barrier reefs. *Cont. Shelf Res.* **2019**, doi:10.1016/j.csr.2019.07.010. [CrossRef]
30. Chevalier, C.; Sous, D.; Devenon, J.L.; Pagano, M.; Rougier, G.; Blanchot, J. Impact of cross-reef water fluxes on lagoon dynamics: A simple parameterization for coral lagoon circulation model, with application to the Ouano Lagoon, New Caledonia. *Ocean. Dyn.* **2015**, 1509–1534. [CrossRef]
31. Symonds, G.; Black, K.P.; Young, I.R. Wave-driven flow over shallow reefs. *J. Geophys. Res. Ocean.* **1995**, *100*, 2639–2648. [CrossRef]

32. Lowe, R.J.; Falter, J.L.; Monismith, S.G.; Atkinson, M.J. Wave-driven circulation of a coastal reef–lagoon system. *J. Phys. Oceanogr.* **2009**, *39*, 873–893. [CrossRef]
33. Pomeroy, A.; Lowe, R.; Symonds, G.; Van Dongeren, A.; Moore, C. The dynamics of infragravity wave transformation over a fringing reef. *J. Geophys. Res. Ocean.* **2012**, *117*, 1–17. [CrossRef]
34. Van Dongeren, A.; Lowe, R.; Pomeroy, A.; Trang, D.M.; Roelvink, D.; Symonds, G.; Ranasinghe, R. Numerical modeling of low-frequency wave dynamics over a fringing coral reef. *Coast. Eng.* **2013**, *73*, 178–190. [CrossRef]
35. Buckley, M.; Lowe, R.; Hansen, J. Evaluation of nearshore wave models in steep reef environments. *Ocean Dyn.* **2014**, *64*, 847–862. [CrossRef]
36. Zijlema, M. Modelling wave transformation across a fringing reef using SWASH. *Coast. Eng. Proc.* **2012**, *1*, 26. [CrossRef]
37. Lashley, C.H.; Roelvink, D.; van Dongeren, A.; Buckley, M.L.; Lowe, R.J. Nonhydrostatic and surfbeat model predictions of extreme wave run-up in fringing reef environments. *Coast. Eng.* **2018**, *137*, 11–27. [CrossRef]
38. Roeber, V.; Cheung, K.F. Boussinesq-type model for energetic breaking waves in fringing reef environments. *Coast. Eng.* **2012**, *70*, 1–20. [CrossRef]
39. Su, S.F.; Ma, G. Modeling two-dimensional infragravity motions on a fringing reef. *Ocean Eng.* **2018**, *153*, 256–267. [CrossRef]
40. Liu, W.; Shao, K.; Ning, Y. A Study of the Maximum Momentum Flux in the Solitary Wave Run-Up Zone over Back-Reef Slopes Based on a Boussinesq Model. *J. Mar. Sci. Eng.* **2019**, *7*, 109. [CrossRef]
41. Roelvink, D.; Reniers, A.; Van Dongeren, A.; de Vries, J.v.T.; McCall, R.; Lescinski, J. Modelling storm impacts on beaches, dunes and barrier islands. *Coast. Eng.* **2009**, *56*, 1133–1152. [CrossRef]
42. Walstra, D.; Roelvink, J.; Groeneweg, J. 3D calculation of wave-driven cross-shore currents. In Proceedings of the 27th International Conference on Coastal Engineering, Sydney, Australia, 16–21 July 2000; pp. 16–21.
43. Holthuijsen, L.; Booij, N.; Herbers, T. A prediction model for stationary, short-crested waves in shallow water with ambient currents. *Coast. Eng.* **1989**, *13*, 23–54. [CrossRef]
44. Janssen, T.; Battjes, J. A note on wave energy dissipation over steep beaches. *Coast. Eng.* **2007**, *54*, 711–716. [CrossRef]
45. Sous, D.; Chevalier, C.; Devenon, J.L.; Blanchot, J.; Pagano, M. Circulation patterns in a channel reef–lagoon system, Ouano lagoon, New Caledonia. *Estuar. Coast. Shelf Sci.* **2017**, *196*, 315–330. [CrossRef]
46. Péquignet, A.C.; Becker, J.; Merrifield, M.; Boc, S. The dissipation of wind wave energy across a fringing reef at Ipan, Guam. *Coral Reefs* **2011**, *30*, 71–82. [CrossRef]
47. Yao, Y.; Zhang, Q.; Chen, S.; Tang, Z. Effects of reef morphology variations on wave processes over fringing reefs. *Appl. Ocean Res.* **2019**, *82*, 52–62. [CrossRef]
48. Dodet, G.; Bertin, X.; Taborda, R. Wave climate variability in the North-East Atlantic Ocean over the last six decades. *Ocean Model.* **2010**, *31*, 120–131. [CrossRef]
49. Charles, E.; Idier, D.; Thiébot, J.; Le Cozannet, G.; Pedreros, R.; Ardhuin, F.; Planton, S. Present wave climate in the Bay of Biscay: Spatiotemporal variability and trends from 1958 to 2001. *J. Clim.* **2012**, *25*, 2020–2039. [CrossRef]
50. Longuet-Higgins, M.S.; Stewart, R. Radiation stress and mass transport in gravity waves, with application to 'surf beats'. *J. Fluid Mech.* **1962**, *13*, 481–504. [CrossRef]
51. Isebe, D.; Azerad, P.; Bouchette, F.; Ivorra, B.; Mohammadi, B. Shape optimization of geotextile tubes for sandy beach protection. *Int. J. Numer. Methods Eng.* **2008**, *74*, 1262–1277. [CrossRef]
52. Vermaak, H.J.; Kusakana, K.; Koko, S.P. Status of micro-hydrokinetic river technology in rural applications: A review of literature. *Renew. Sustain. Energy Rev.* **2014**, *29*, 625–633. [CrossRef]
53. Khan, M.; Iqbal, M.; Quaicoe, J. River current energy conversion systems: Progress, prospects and challenges. *Renew. Sustain. Energy Rev.* **2008**, *12*, 2177–2193. [CrossRef]
54. Ibarra-Berastegi, G.; Sáenz, J.; Ulazia, A.; Serras, P.; Esnaola, G.; Garcia-Soto, C. Electricity production, capacity factor, and plant efficiency index at the Mutriku wave farm (2014–2016). *Ocean Eng.* **2018**, *147*, 20–29. [CrossRef]
55. Lehmann, M.; Karimpour, F.; Goudey, C.A.; Jacobson, P.T.; Alam, M.R. Ocean wave energy in the United States: Current status and future perspectives. *Renew. Sustain. Energy Rev.* **2017**, *74*, 1300–1313. [CrossRef]
56. Zhou, Z.; Benbouzid, M.; Charpentier, J.F.; Scuiller, F.; Tang, T. Developments in large marine current turbine technologies—A review. *Renew. Sustain. Energy Rev.* **2017**, *71*, 852–858. [CrossRef]

57. Bouvier, C.; Castelle, B.; Balouin, Y. Modeling the Impact of the Implementation of a Submerged Structure on Surf Zone Sandbar Dynamics. *J. Mar. Sci. Eng.* **2019**, *7*, 117. [CrossRef]
58. Duarte Nemes, D.; Fabián Criado-Sudau, F.; Nicolás Gallo, M. Beach Morphodynamic Response to a Submerged Reef. *Water* **2019**, *11*, 340. [CrossRef]
59. Isebe, D.; Azerad, P.; Mohammadi, B.; Bouchette, F. Optimal shape design of defense structures for minimizing short wave impact. *Coast. Eng.* **2008**, *55*, 35–46. [CrossRef]